

Observation of a time crystal comb in a driven-dissipative system with Rydberg gas

Yuechun Jiao^{1,3†}, Weilun Jiang^{2,3†}, Yu Zhang¹, Jingxu Bai¹,
Yunhui He¹, Heng Shen^{2,3*}, Jianming Zhao^{1,3*}, Suotang Jia^{1,3}

¹State Key Laboratory of Quantum Optics and Quantum Optics Devices,
Institute of Laser Spectroscopy, Shanxi University, Taiyuan, 030006, China

²Institute of Opto-Electronics, Shanxi University, Taiyuan, 030006, China

³Collaborative Innovation Center of Extreme Optics
Shanxi University, Taiyuan, 030006, China

*Corresponding authors; e-mail: hengshen@nbi.dk, zhaojm@sxu.edu.cn

[†]These authors contributed equally to this work.

April 16, 2024

Time crystals, as temporal analogs of space crystals, manifest as stable and periodic behavior that breaks time translation symmetry. In an open quantum system, many-body interaction subjected to dissipation allows one to develop the time crystalline order in an unprecedented way, as refer to dissipative time crystal. Here we report the observation of a time crystal comb in the continuously driven-dissipative and strongly interacting Rydberg thermal gas, in which continuous time crystal and sub-harmonics of limit cycles as well as the high-order harmonic oscillation phases are observed in the same system by manipulating the Rydberg excitation. Our work provides new ways to explore the nonequilibrium phases of matter in open systems. Such time crystals with persistent oscillation rooted in emergent quantum correlations, may emerge as a ubiquitous tool in quantum metrology, for instance, continuous sensing and parameter estimation surpassing the standard quantum limit.

Crystal is a collection of atoms with the periodic arrangement in space, a celebrated

example of spontaneous spatial translation symmetry breaking, ranging from salt and jewelry in the daily life to bulk materials in the condensed matter experiment. We are accustomed to an inherent impression that time is on an equal footing with space, are thus curious whether time-translation symmetry can be spontaneously broken to form a time crystal. The original proposal of continuous time crystal (CTC) for isolated many-body systems in equilibrium [1] is prohibited by no-go theorems [2, 3]. Instead, discrete time crystals (DTC) undergoing the spontaneous breaking of discrete time translation symmetry were discovered by applying a periodic external drive in an interacting many-body system under the ergodicity breaking. Such a closed system features a subharmonic response [4, 5, 6, 7, 8, 9], and the associated time crystalline order is stabilized by disorder-induced many-body localization [10, 11, 7] or prethermalization due to sufficiently high Floquet drive frequency [6, 12].

An alternate strategy to stabilize the time crystalline order is dissipation [13, 14, 15, 16, 17, 18, 19, 20], which is conventionally believed to destroy the order. Similar to reservoir engineering for preparing the desired quantum states, the discrete time crystalline order in a driven open Dicke model was realized by tailoring system-environment coupling appropriately [21, 22, 23]. Remarkably, following the pioneering theoretical works [24, 15], a limit cycle phase without a recurring external force has also been confirmed recently in the platform of dissipative-driven Dicke model with ultra-cold atoms inside an optical cavity [25]. As the manifestation of CTC, a persistent oscillation robust against temporal perturbations was observed, taking the random phase between 0 and 2π for different realizations [25, 26]. In view of the foregoing, it is natural to raise a question, whether the interplay of strong interaction, dissipation and synchronization in the non-equilibrium open system could further enrich dynamic phases that spontaneously break time translation symmetry.

Here, we report the observation of a complex time crystalline order in the dissipative Rydberg gas at room temperature, exhibiting a series of spontaneous self-sustained oscillations of limit cycles under the time-independent external driving. Going beyond an inherent continuous time crystal phase, we surprisingly find sub-harmonic and high-order harmonic oscillations of limit cycles emerge successively in this open, quantum many-body system, regarded as discrete time crystalline order and nonlinearity induced high-order harmonics, respectively. This is distinct from recent observation of CTC [27], a transient oscillation [28] and synchronized oscillation [29] in limit cycles with continuously driven Rydberg gas. Our work thus provides new understandings about a rich interplay between interaction, dissipation and synchronization in a quantum many-body system under continuous monitoring.

We consider an ensemble of Rydberg atoms at room temperature. As illustrated in Fig. 1 a, two laser beams, referred to as probe and control, excite the ground state $|g\rangle$ to the Rydberg state $|r\rangle$ via an intermediate state $|e\rangle$. This forms a ladder-type electromagnetically

induced transparency (EIT) configuration, and the associated strong interaction is given by the Hamiltonian $\hat{H}_I = \sum_{j < k} V_{jk} \hat{n}_j \hat{n}_k$ with the local Rydberg density \hat{n}_j and the van der Waals interaction $V_{jk} \propto -C_6/|\vec{r}_j - \vec{r}_k|^6$ between Rydberg atoms located at \vec{r}_j and \vec{r}_k , with C_6 the dispersive coefficient ($C_6 < 0$ for cesium $60D_{5/2}$ atom used here). To take the spontaneous emission into account through the dissipative term, dissipation is embodied in the Lindblad master equation, $\dot{\rho} = \mathcal{L}(\rho)$, and

$$\mathcal{L}(\rho) = -i[\hat{H}, \rho] + \Gamma \sum_j \left(\hat{\sigma}_j \rho \hat{\sigma}_j^\dagger - \frac{1}{2} \left\{ \hat{\sigma}_j^\dagger \hat{\sigma}_j, \rho \right\} \right). \quad (1)$$

$\hat{\sigma}_j = |g_j\rangle \langle r_j|$ is the jump operator between ground and Rydberg state on site j . In a thermal Rydberg gas, the mean-field approach is usually employed to describe the interaction [30, 31] (see Supplementary materials for more details). Strong interaction and nonlinearity competing with dissipation offer the opportunities for exploring exotic non-equilibrium many-body phases, such as optical bistability [30], self-organized criticality [32] and the transition towards synchronization [29].

To experimentally observe the non-equilibrium phases of matter in thermal Rydberg gas, we use a resonant two-photon excitation scheme in a Cesium vapor cell at room temperature. The counter-propagating probe (852 nm, Ω_p) and control (509 nm, Ω_c) fields set up the Rydberg EIT process (Fig. 1a). A magnetic field $B = 11.8$ G along the propagation direction is applied to induce the large Zeeman splitting, thus ensuring the exact Zeeman level of the involving states can be specified by the polarization of the beams (See the Methods). In this work, two laser beams with σ^+ circular polarization excite the transition of $|g\rangle = |6S_{1/2}, F = 4, m_F = 4\rangle$ to $|r\rangle = |60D_{5/2}, m_j = 5/2\rangle$ via the intermediate state $|e\rangle = |6P_{3/2}, F' = 5, m'_F = 5\rangle$ with detuning of $\delta_p = 2\pi \times 70$ MHz. A differential detection is used to suppress the laser intensity noise.

For a driven-dissipative system such as Rydberg gas, strong interaction-induced nonlinearity results in the multistability of the equations of motion [30, 32]. Hence, a Hopf bifurcation occurs when a complex conjugate pair of eigenvalues cross the imaginary axis with non-zero speed as varying the parameter [29]. The resulting steady state becomes unstable, where the non-zero imaginary part causes to the oscillation between various stable states. As a consequence, the system is attracted to the limit circle with a persistent oscillation, instead of the fix point, described by the stable solution in equilibrium.

On the experimental side, the high degree of controllability on Rydberg excitation facilitates the observation of phases in the limit cycle. Here we perform a scanning EIT spectroscopy measurement by engineering the Rydberg excitation in terms of Rabi frequencies of control field, Ω_c . Below a certain value of Ω_c , normal EIT spectra are observed, while optical bistable phase emerges if exceeding it. By increasing Ω_c further, we observe oscillations of the transmission signal at the range of two-photon detuning $\Delta/2\pi \sim 30$ -40 MHz,

and Fig. 1b displays a typical transmission EIT spectrum exhibiting self-sustained oscillation. Insets illustrate a typical realization of spontaneous self-sustained oscillation in this parameter region ($\Delta = 2\pi \times 36$ MHz). The associated normalized single-sided amplitude spectra $A(\omega)$ is shown in the right panel. A narrow peak at $\omega_{LC}/2\pi = 8.56$ kHz with the full width at half maximum of 0.05 kHz (a time window of 16 ms) suggests a stable periodic oscillation pattern. In addition, a single-shot realization of quench dynamics is shown in the Fig. S7, where the probe field is suddenly switched on and then held at a constant power for a long time (280 ms). After a short time establishment, this persistent oscillation is sustained in the entire probing duration.

We stress that only single Rydberg state, $|60D_{5/2}, m_j = 5/2\rangle$, is involved in the driving scheme since we select the configuration of Rydberg transition via laser polarization, which distinguishes our finding sharply from the recent work [27] where the appearance of oscillations is attributed to a competition of multiple Rydberg states. Scanned transmission spectra for the different polarization are plot in Extended Data Fig. 1.

As defined, the spontaneous breaking of continuous time translation symmetry and robustness against temporal perturbations constitute the essence of continuous time crystal. In Fig. 1c, we show the time phase of oscillations are randomly distributed over $[0, 2\pi]$ for 250 independent realizations, indicative of a spontaneous breaking of continuous time translation symmetry. Regarding a characterization of the robustness, we apply a white noise onto the probe beam, and use the relative crystalline fractions Ξ to describe the robustness of the CTC on the noise strength N [25]. The relative crystalline fractions and the noise strength N are defined by $\Xi = \Sigma_{\omega=\omega_{LC}\pm\delta\omega}|A(\omega)|/\Sigma_{\omega}|A(\omega)|$ and $N = \Sigma_{\omega}|P_n(\omega)|/\Sigma_{\omega}|P_0(\omega)| - 1$, respectively. $\delta\omega$ denotes the resolution of the single-sided amplitude, P_n and P_0 are the single-sided amplitude spectrum of the probe laser with and without white noise. Fig. 1d shows the measured crystalline fraction as a function of the noise strength N . It exists over a wide parameter range, indicating the limit cycle phase is insensitive to the temporal perturbations.

We would like to emphasize that CTC or limit cycle phase in thermal Rydberg gas was recently reported by three other groups [27, 28, 29], however, a substantial issue, the dependence of oscillation frequency, is unrevealed so far. To circumvent this limitation, we thus explicitly leverage the concept of boundary time crystal (BTC) [24]. As a paradigmatic example of continuous dissipative time crystal, an oscillatory phase there is induced by the interplay of driving and dissipation, and the associated frequency scales linearly as Ω/Γ with the coherent interaction strength Ω and the dissipation rate Γ . In the BTC scenario, the interacting many-body system and the environment are interpreted as bulk and boundary, respectively. At first, we confirm that our system indeed falls into the category of BTC via Liouvillian spectrum. Figs. 1e and f present the eigenvalues of the Liouvillian with parameters in (out of) the oscillation phase. Ignoring the finite size effect, we iden-

tify gapless spectrum and a non-zero imaginary part displayed in Fig. 1e as an signature of BTC [24]. Here, a non-zero imaginary part of the Liouvillian spectrum induces the persistent oscillation.

We proceed to investigate the dependence of oscillation frequency by varying the Rabi frequency of control field. Given the fixed Rabi frequency of probe field and bias magnetic field, the experimental result shows the oscillation frequency is linearly proportional to the coupling laser Rabi frequency, shown in Fig. 1g, in agreement with the simulated results qualitatively (Fig. 1h).

To explore the CTC phase further and probe the boundary of this phase, we slightly increase the coupling laser Rabi frequency Ω_c from $2\pi \times 2.29$ MHz to $2\pi \times 2.84$ MHz. Surprisingly, we find another persistent periodic oscillation at lower frequency in the scanned transmission EIT spectrum (Fig. 2b). By analysing the frequency of two oscillation components with fixed the coupling laser detuning to $\Delta = 2\pi \times 50$ MHz (the purple circle point) and $2\pi \times 70$ MHz, we find the new emergent oscillation has a frequency of 4.38 kHz (inset left panel in Fig. 2b) that is a half of the CTC oscillations, 9.07 kHz (inset right panel in Fig. 2b). We also test the robustness of the limit cycle to rule out the possibility of classical nonlinearity, shown in Fig. 2c.

To understand such a spontaneous period-doubling phenomenon, we endeavour to develop a physical picture from the theoretical point of view (Fig. 2a). In contrast with DTC in periodically driven closed systems where disorder-induced many-body localization or prethermalization stabilize the crystalline order, we emphasize that our original system Hamiltonian is absence of disorder, easily thermalized, and time-independent. More importantly, there exists metastability in respect to Rydberg population. Drawing inspiration from the recent discovery [17], we attribute this feature to the combination of a periodic driving raised by the stable oscillation of Rydberg populations, and the nonlinearity induced optical bistability, in form of dissipative DTC. In addition, we assume the periodic driving comes from the steady oscillation of Rydberg population induced by CTC phase, resulting in the random distribution of its time phase, as shown in Fig. 2d (See Supplementary Materials for more details).

As a matter of fact, nonlinearity becomes crucial and thereby alter the oscillation as the Rydberg interaction dominates the dynamics. Similar to optical Kerr effect, we intuitively expect that under the nonlinear Hamiltonian, higher-order harmonics appear if exceeding a certain threshold. Experimentally, when lifting the Rabi frequency up to $2\pi \times 4.93$ MHz, the scanned transmission EIT spectrum manifests emergent higher-order harmonics (labeled with f_1 and f_2), in addition to the CTC and DTC oscillations (labeled with f and $f/2$), shown in Fig. 3a. We extract their oscillation frequencies by discrete Fourier transform with a time window of 16 ms, giving the values of 50.71 kHz, 20.23 kHz, 6.02 kHz, and 12.13 kHz, respectively, roughly corresponding to $f_2 \approx 4f$, $f_1 \approx 3f/2$, $f/2$

and f . Subsequently, random distributions of their time phase with 250 repeated realizations are observed (Figs. 3b-e), demonstrating the higher harmonics of limit cycle phases. The resulting dynamic in this case is determined solely by the intrinsic nonlinearity of the Rydberg gas.

In conclusion, we report the observation of a complex time crystalline order in an ensemble of thermal Rydberg gas under the continuous drive. The observed self-sustained oscillations are recognized as continuous time crystal, discrete time crystal and higher-order harmonics. As an intrinsically out-of-equilibrium system, it provides a simple but versatile platform for exploring the exotic dynamic phases of open quantum system [33, 34, 35, 36], such as macroscopic quantum synchronization effect [37, 38]. As suggested by recent work [39], time crystals observed here may be exploited in quantum metrology, such as continuous sensing surpassing the standard quantum limit [40], and time crystalline order as a frequency standard [41].

References

- [1] Wilczek, F. Quantum time crystals. *Physical Review Letters* **109**, 160401 (2012).
- [2] Bruno, P. Impossibility of spontaneously rotating time crystals: A no-go theorem. *Physical Review Letters* **111**, 070402 (2013).
- [3] Watanabe, H. & Oshikawa, M. Absence of quantum time crystals. *Physical Review Letters* **114**, 251603 (2015).
- [4] Pal, S., Nishad, N., Mahesh, T. S. & Sreejith, G. J. Temporal order in periodically driven spins in star-shaped clusters. *Physical Review Letters* **120**, 180602 (2018).
- [5] Smits, J., Liao, L., Stoof, H. T. C. & Van Der Straten, P. Observation of a space-time crystal in a superfluid quantum gas. *Physical Review Letters* **121**, 185301 (2018).
- [6] Kyprianidis, A. *et al.* Observation of a prethermal discrete time crystal. *Science* **372**, 1192–1196 (2021).
- [7] Randall, J. *et al.* Many-body-localized discrete time crystal with a programmable spin-based quantum simulator. *Science* **374**, 1474–1478 (2021).
- [8] Mi, X. *et al.* Time-crystalline eigenstate order on a quantum processor. *Nature* **601**, 531–536 (2022).
- [9] Zhang, X. *et al.* Digital quantum simulation of floquet symmetry-protected topological phases. *Nature* **607**, 468–473 (2022).

- [10] Zhang, J. *et al.* Observation of a discrete time crystal. *Nature* **543**, 217–220 (2017).
- [11] Choi, S. *et al.* Observation of discrete time-crystalline order in a disordered dipolar many-body system. *Nature* **543**, 221–225 (2017).
- [12] Vu, D. & Das Sarma, S. Dissipative Prethermal Discrete Time Crystal. *Physical Review Letters* **130**, 130401 (2023).
- [13] Chitra, R. & Zilberberg, O. Dynamical many-body phases of the parametrically driven, dissipative Dicke model. *Physical Review A* **92**, 023815 (2015).
- [14] Gong, Z., Hamazaki, R. & Ueda, M. Discrete time-crystalline order in cavity and circuit qed systems. *Physical Review Letters* **120**, 040404 (2018).
- [15] Buča, B., Tindall, J. & Jaksch, D. Non-stationary coherent quantum many-body dynamics through dissipation. *Nature Communications* **10**, 1730 (2019).
- [16] Zhu, B., Marino, J., Yao, N. Y., Lukin, M. D. & Demler, E. A. Dicke time crystals in driven-dissipative quantum many-body systems. *New Journal of Physics* **21**, 073028 (2019).
- [17] Gambetta, F. M., Carollo, F., Marcuzzi, M., Garrahan, J. P. & Lesanovsky, I. Discrete Time Crystals in the Absence of Manifest Symmetries or Disorder in Open Quantum Systems. *Physical Review Letters* **122**, 015701 (2019).
- [18] Booker, C., Buča, B. & Jaksch, D. Non-stationarity and dissipative time crystals: Spectral properties and finite-size effects. *New Journal of Physics* **22**, 085007 (2020).
- [19] Yao, N. Y., Nayak, C., Balents, L. & Zaletel, M. P. Classical discrete time crystals. *Nature Physics* **16**, 438–447 (2020).
- [20] Alaeian, H., Giedke, G., Carusotto, I., Löw, R. & Pfau, T. Limit cycle phase and Goldstone mode in driven dissipative systems. *Physical Review A* **103**, 013712 (2021).
- [21] Keßler, H. *et al.* Observation of a dissipative time crystal. *Physical Review Letters* **127**, 043602 (2021).
- [22] Kongkhambut, P. *et al.* Realization of a periodically driven open three-level dicke model. *Physical Review Letters* **127**, 253601 (2021).
- [23] Taheri, H., Matsko, A. B., Maleki, L. & Sacha, K. All-optical dissipative discrete time crystals. *Nature Communications* **13**, 848 (2022).

- [24] Iemini, F. *et al.* Boundary time crystals. *Physical Review Letters* **121**, 035301 (2018).
- [25] Kongkhambut, P. *et al.* Observation of a continuous time crystal. *Science* **377**, 670–673 (2022).
- [26] Chen, Y.-H. & Zhang, X. Realization of an inherent time crystal in a dissipative many-body system. *Nature Communications* **14**, 6161 (2023).
- [27] Wu, X. *et al.* Observation of a dissipative time crystal in a strongly interacting rydberg gas. *arXiv:2305.20070* (2023).
- [28] Ding, D. *et al.* Ergodicity breaking from Rydberg clusters in a driven-dissipative many-body system. *Science Advances* **10**, ead15893 (2024).
- [29] Wadenpfuhl, K. & Adams, C. S. Emergence of synchronization in a driven-dissipative hot rydberg vapor. *Physical Review Letters* **131**, 143002 (2023).
- [30] Carr, C., Ritter, R., Wade, C. G., Adams, C. S. & Weatherill, K. J. Nonequilibrium phase transition in a dilute rydberg ensemble. *Physical Review Letters* **111**, 113901 (2013).
- [31] Marcuzzi, M., Levi, E., Diehl, S., Garrahan, J. P. & Lesanovsky, I. Universal Nonequilibrium Properties of Dissipative Rydberg Gases. *Physical Review Letters* **113**, 210401 (2014).
- [32] Ding, D.-S., Busche, H., Shi, B.-S., Guo, G.-C. & Adams, C. S. Phase diagram and self-organizing dynamics in a thermal ensemble of strongly interacting rydberg atoms. *Physical Review X* **10**, 021023 (2020).
- [33] Saffman, M., Walker, T. G. & Mølmer, K. Quantum information with Rydberg atoms. *Rev. Mod. Phys.* **82** (2010).
- [34] Pizzi, A., Knolle, J. & Nunnenkamp, A. Period- n discrete time crystals and quasicrystals with ultracold bosons. *Phys. Rev. Lett.* **123**, 150601 (2019).
- [35] Yang, X. & Cai, Z. Dynamical transitions and critical behavior between discrete time crystal phases. *Phys. Rev. Lett.* **126**, 020602 (2021).
- [36] Bakker, L. R. *et al.* Driven-Dissipative Time Crystalline Phases in a Two-Mode Bosonic System with Kerr Nonlinearity. *Physical Review Letters* **129**, 250401 (2022).

- [37] Nadolny, T. & Bruder, C. Macroscopic Quantum Synchronization Effects. *Physical Review Letters* **131**, 190402 (2023).
- [38] Hajdušek, M., Solanki, P., Fazio, R. & Vinjanampathy, S. Seeding Crystallization in Time. *Physical Review Letters* **128**, 080603 (2022).
- [39] Choi, S., Yao, N. & Lukin, M. Quantum metrology based on strongly correlated matter. *arXiv.1801.00042* (2017).
- [40] Cabot, A., Carollo, F. & Lesanovsky, I. Continuous sensing and parameter estimation with the boundary time crystal. *Phys. Rev. Lett.* **132**, 050801 (2024).
- [41] Lyu, C., Choudhury, S., Lv, C., Yan, Y. & Zhou, Q. Eternal discrete time crystal beating the heisenberg limit. *Phys. Rev. Res.* **2**, 033070 (2020).
- [42] Lee, T. E., Häffner, H. & Cross, M. C. Antiferromagnetic phase transition in a nonequilibrium lattice of rydberg atoms. *Phys. Rev. A* **84**, 031402 (2011).

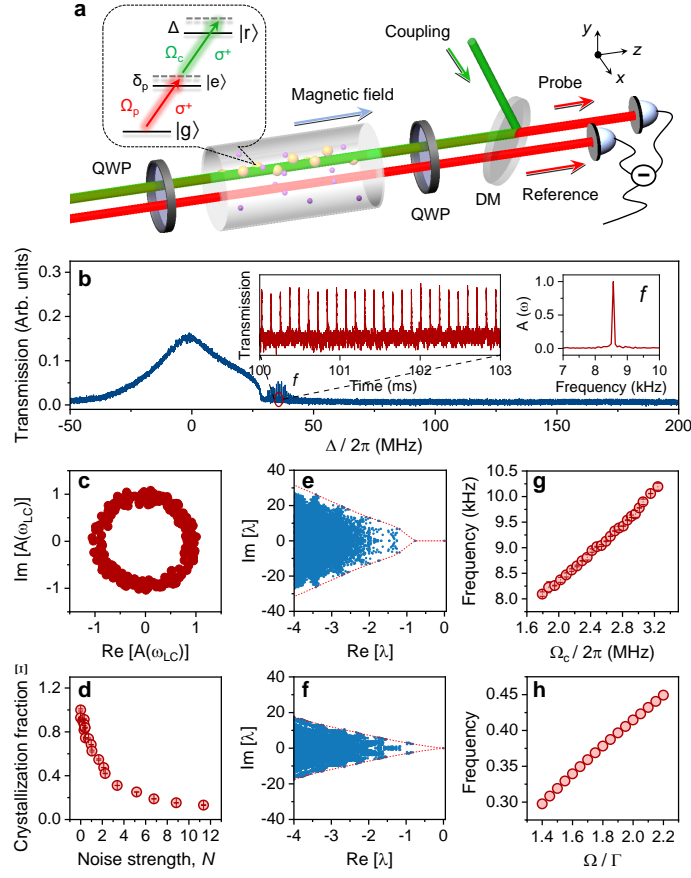


Figure 1: Emergence of continuous time crystal in a continuously driven-dissipative Rydberg system. **a**, Schematic of the experimental setup and relevant energy level. QWP: quarter-wave plate, DM: dichroic mirror. **b**, Scanned transmission spectrum with $\Omega_p = 2\pi \times 24.97$ MHz and $\Omega_c = 2\pi \times 2.29$ MHz. Insets show the single-shot realization of the spontaneous self-sustained oscillation for $\Delta = 2\pi \times 36$ MHz and corresponding normalized single-sided amplitude spectra. **c**, Distribution of the time phase in the limit cycle phase 250 independent realizations. **d**, Relative crystalline fraction Ξ as a function of noise strength N . **e**, **f**, Eigenvalues λ of the Liouvillian in (out of) the oscillatory phase for finite size calculation $L = 8$. In particular, we choose the parameters of $(\Delta/\Gamma = 4, V/\Gamma = 5, \Omega/\Gamma = 2)$ for **e**, and $(\Delta/\Gamma = 2.5, V/\Gamma = 5, \Omega/\Gamma = 2.5)$ for **f**. The sole eigenvalues located on the real axis closed to zero show the gapped feature outside of the oscillatory phase. While, in **f**, all the eigenvalues located on the real axis possess commensurate eigenvalues with imaginary part, indicating the non-trivial oscillations. **g**, Measurements of the oscillations frequency of CTC as a function of coupling Rabi frequency Ω_c . **h**, Simulated oscillations frequency of the time crystal according to the Hamiltonian in Eq. (2), with $\Delta/\Gamma = 2$ and $V/\Gamma = 5$.

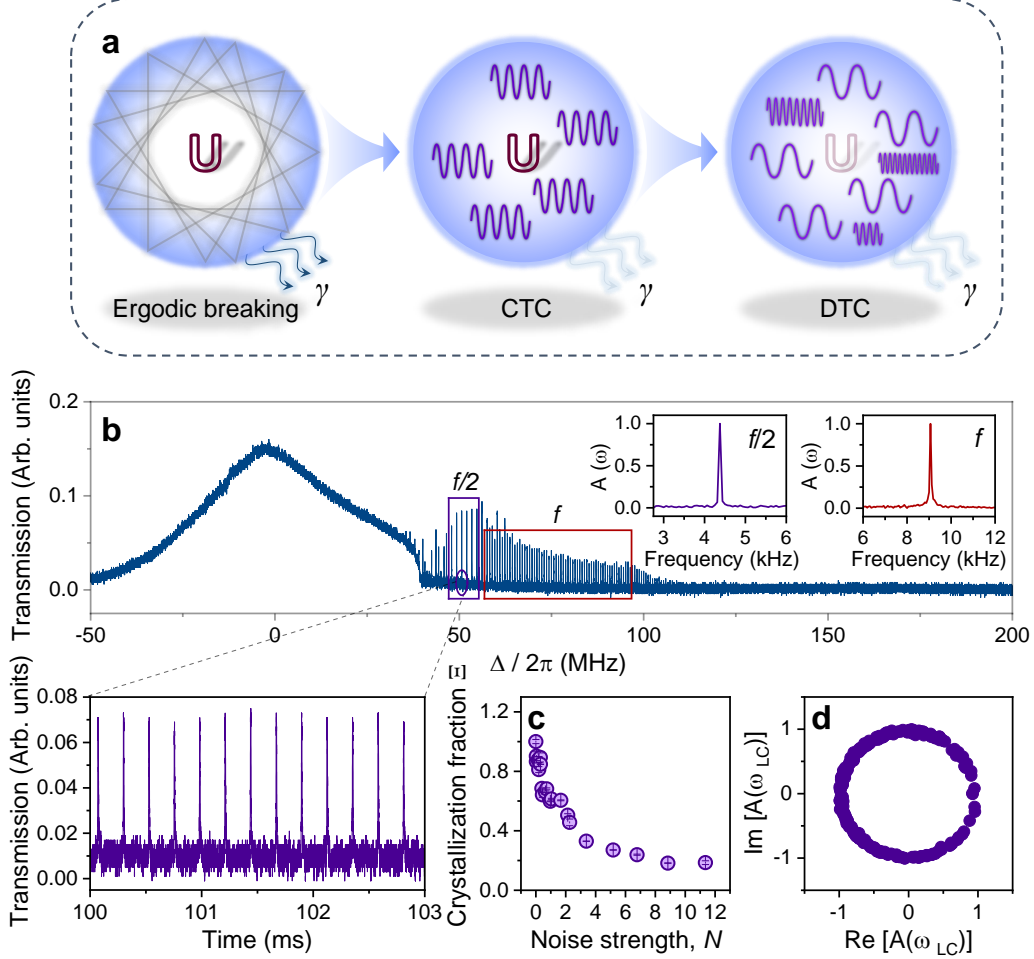


Figure 2: **Observation of a self-sustained subharmonic oscillation.** **a**, Illustration of the mechanism for developing dissipative continuous and discrete time crystals. **b**, Scanned transmission spectrum with $\Omega_c = 2\pi \times 2.84$ MHz. Inset: discrete Fourier transformation of the self-sustained oscillations in parameter region marked in violet and red, respectively. **c**, Robustness of the observed subharmonic oscillation pattern. **d**, Distribution of the time phase in the limit cycle phase.

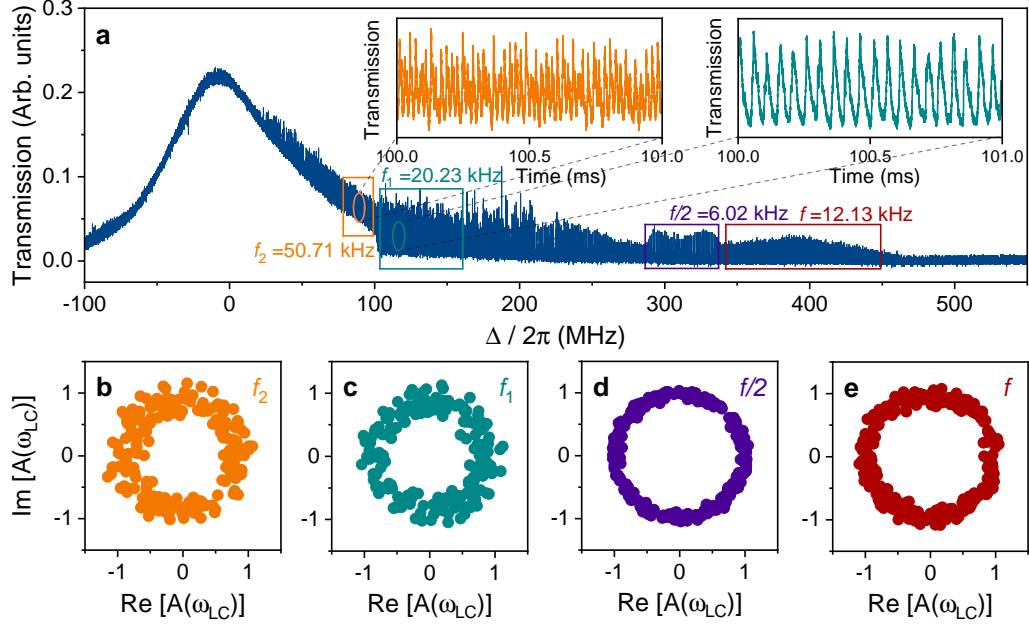


Figure 3: **Nonlinearity induced high order harmonics.** **a**, Scanned transmission spectrum with $\Omega_c = 2\pi \times 4.93$ MHz. Continuous time crystal, subharmonic and high-order harmonics (denote as f , $f/2$, $f_1 \approx 3f/2$ and $f_2 \approx 4f$) appear at different detuning, simultaneously. The corresponding oscillation frequencies are obtained by single-sided amplitude spectra. Inset shows the persistent high-order harmonic oscillations with given detunings. **b - e**, The distribution of the time phase in the limit cycle phase for high-order harmonics, subharmonic oscillation, and continuous time crystals.

Methods

Experimental details

The experiment is conducted on a room-temperature Cs vapour cell (with a diameter of 2.5 cm and length of 7.5 cm). The 852 nm and 509 nm lasers are delivered by Toptica DL pro and Precilasers, respectively. High finesse ultralow expansion (ULE) cavities provide the feedback for the frequency stabilization of both laser (FSR: 1.5 GHz, Finesse 1.5×10^5). The tunable offset-lock frequency ensures the measurement of limit cycle phase and robustness with fixed laser detuning. In addition, the 509 nm laser works in frequency-scanning mode for the measurement of scanned EIT transmission spectrum. The $1/e^2$ beam waist of 852 nm and 509 nm are $\omega_p = 425 \mu\text{m}$ and $\omega_c = 450 \mu\text{m}$, respectively. The homogeneous magnetic field B along with the probe direction is generated by a Helmholtz coils with 220 mm inner diameter. A probe and a reference beams pass through two identical acoustic optical modulator (AOM) before entering the cell. When exploring the robustness against temporal perturbations of time crystals, we introduce white noise onto the probe beam by adding the white noise strength to modulate the RF amplitude of AOM, rather than the reference beam.

Selection of Rydberg transition

The exact Zeeman level of the Rydberg states involved, $|r\rangle = |60D_{5/2}, m_j = 5/2\rangle$, is specified by careful choosing the polarization of the excitation beams under the condition of $B = 11.8$ G. The polarization of probe beam is set to σ^+ , while the polarization of coupling beam is tuned with a quarter-wave plate. Extended Data Fig. 1a shows three scanned transmission spectra for different polarization of coupling beam, σ^+ (top panel), elliptical (middle panel) and σ^- (bottom panel). Here, we fix the probe Rabi frequency at $\Omega_p = 2\pi \times 24.97$ MHz and coupling laser power at 16 mW. Subject to the transition selection rule, given the σ^+ polarized coupling beam, only $|r\rangle = |60D_{5/2}, m_j = 5/2\rangle$ Rydberg state can be excited and related EIT signal appear (see top panel of Extended Data Fig. 1a), while for the σ^- case only $|r\rangle = |60D_{5/2}, m_j = 1/2\rangle$ Rydberg EIT can be obtained, as shown in the bottom panel. The elliptical polarized coupling can excite both $|60D_{5/2}, m_j = 5/2\rangle$ and $|60D_{5/2}, m_j = 1/2\rangle$ states, and thereby form two separated EIT signals (middle panel of Extended Data Fig. 1a), one of which locates at $\Delta = -318$ MHz is contributed by $60D_{3/2}$ Rydberg state. In accordance with $60D_{3/2}$ EIT signal, we judiciously tune the polarization of the coupling beam.

By increasing the coupling laser power up to 76 mW, we observe the persistent oscillations for all three polarization setting, as illustrated in Extended Data Fig. 1b.

Evolution of the scanned transmission spectrum at increasing Rabi frequency Ω_c

In order to probe the phase, we measure the transmission spectra by varying the coupling Rabi frequency. Extended Data Fig. 2 displays a series of measured transmission spectrum for different indicated coupling Rabi frequencies Ω_c (marked in the panels). Here we set $\Omega_p = 2\pi \times 24.97$ MHz and $B = 11.8$ G. We clearly see that an oscillation with the frequency of f appears firstly at $\Omega_c = 2\pi \times 2.19$ MHz. By slightly increasing Ω_c up to $2\pi \times 2.39$ MHz, an subharmonic oscillation with the frequency of $f/2$ emerges together with the f frequency component. As further increasing the Rabi frequency Ω_c , high frequency oscillations appear and we observe CTC, DTC and higher-order harmonics simultaneously. The transmission signal between f_1 and $f/2$ components is unstable with the ill-defined period which cannot maintain their shape.

Mean-field analysis and Liouvillian spectrum

In this section, we consider two-level system of Rydberg-type Hamiltonian,

$$\hat{H} = \sum_j [-\Delta(t)\hat{n}_j + \Omega(t)\hat{\sigma}_j^x] + \sum_{j < k} V_{jk}\hat{n}_j\hat{n}_k, \quad (2)$$

where Δ and Ω are the laser detuning and Rabi frequency, while V represents the van der Waals interaction between two Rydberg atoms. Besides, dissipation is embodied in the Lindblad master equation, $\dot{\rho} = \mathcal{L}(\rho)$, written in Eq.(1).

In the thermal Rydberg gas, the mean-field method is usually utilized. Initially, one may consider the uniform Rydberg population at each site, $\langle n_i \rangle = \langle n \rangle$. It is proved that under such a condition, no Hopf bifurcation occurs. The oscillation between the ground state and the Rydberg state is thus absent[29]. Next, one could divide the total Rydberg atoms into two uniform parts. Here, an oscillation phase with respect to the Rydberg population for bipartite subsystem is identified [42]. By numerically solving non-linear Bloch equation with Runge-Kutta method, we extract the frequency (See Supplementary Materials for more details).

To make comparison with the experiment, we fix the detuning and Rydberg interactions and vary the Rabi to extract the oscillatory frequency, given that we are in the oscillation phase. In Fig. 1h, we find the similar linear behaviour as the experiment result.

The Liouvillian spectrum is the collection of all eigenvalues of Liouvillian supermatrix. Since the master equation writes, $\dot{\rho} = \mathcal{L}(\rho)$, the Liouvillian acts on the density matrix instead of a vector, thus is referred to as superoperator. The density matrix $\hat{\rho}$ can be linearization as an vector $|\rho\rangle$, and the Liouvillian possess a matrix form. We diagonalize such

Liouvillian superoperator and draw the spectrum in Figs. 1e, f.

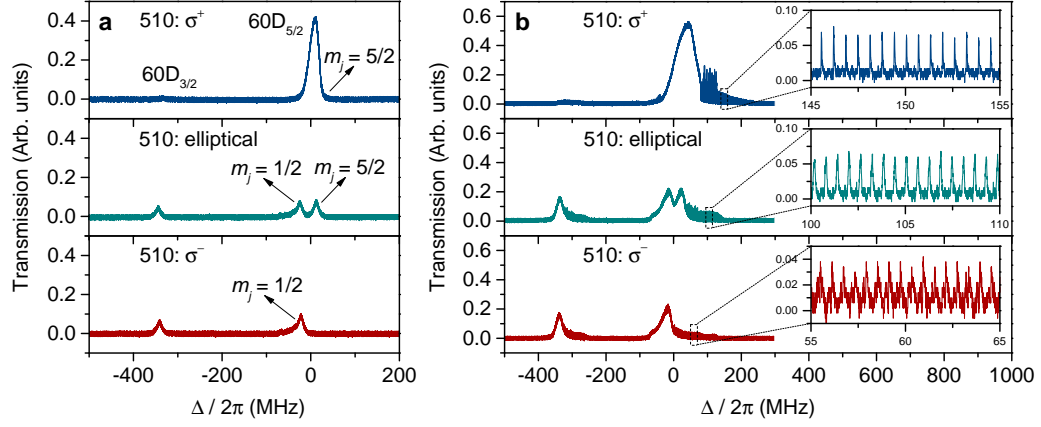
Data availability The data are available from the corresponding author on reasonable request.

Code availability The codes are available upon reasonable request from the corresponding author.

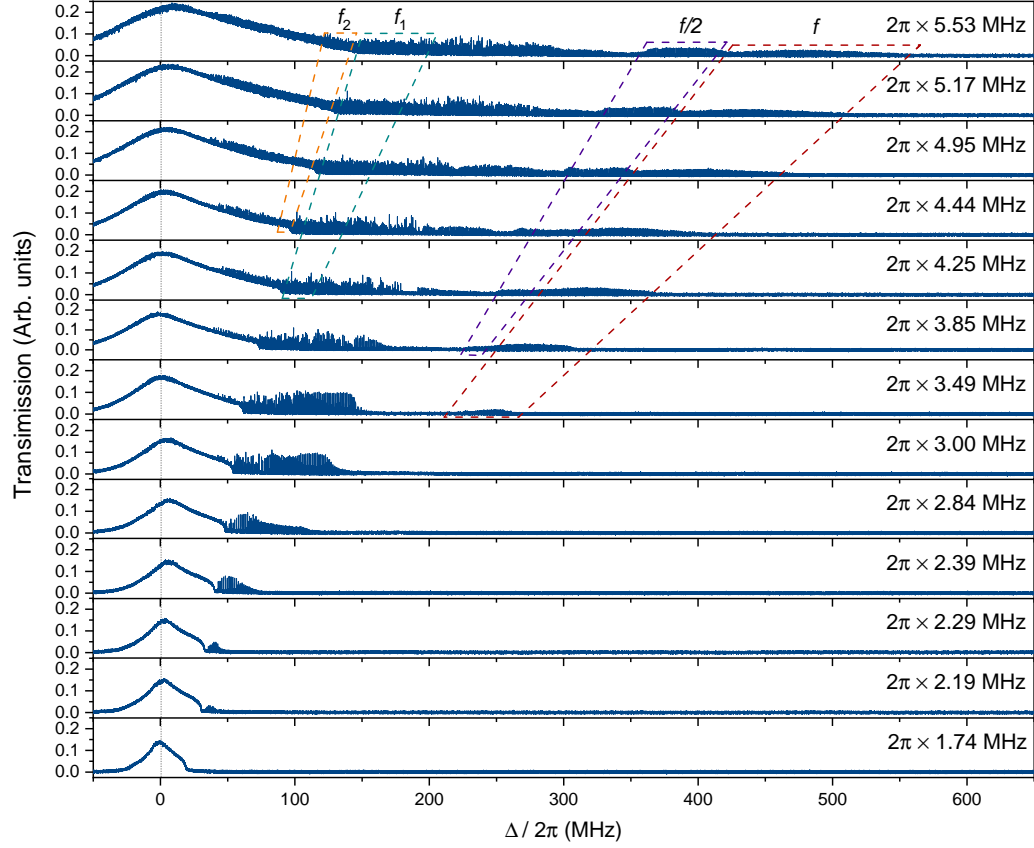
Acknowledgements This work was supported by the National Key R&D Program of China (grant no. 2020YFA0309400), and NSFC of China (grant no. U2341211, 12241408, 62175136, 12120101004 and 12222409). H. S. acknowledges financial support from the Royal Society Newton International Fellowship Alumni follow-on funding (AL201024) of the United Kingdom.

Author contributions Y.J., H.S. and J.Z. conceived the idea. Y.J., Y.Z, and J.B. performed the experiment and collected the data. W.J., Y.H. and H.S. contributed to the data analysis. Y.J., W.J., H.S., J.Z. and S. J. wrote the manuscript with contribution from all authors.

Competing interests The authors declare no competing interests.



Extended Data Fig. 1: **a**, Scanned transmission spectra for three indicated coupling laser polarization and σ^+ polarization of probe beam, magnetic field $B = 11.8$ G and coupling laser is 16 mW. **b**, The scanned transmission spectra with increasing coupling laser power to 76 mW. Inset shows an enlargement of time crystal.



Extended Data Fig. 2: Dynamic of the scanned transmission spectra for indicated Rabi frequency Ω_c and $\Omega_p = 2\pi \times 24.97$ MHz and $B = 11.8$ G. The colored zone lines mark the oscillation region with indicated frequencies f , $f/2$, f_1 and f_2 when the Ω_c vary from $2\pi \times 3.49$ MHz to $2\pi \times 5.53$ MHz.